Title
PION-MASS MEASUREMENT BY CRYSTAL DIFFRACTION OF MESONIC X RAYS

Author
Shafer, Robert E.

Publication Date
1967-11-02

UCRL-16638

University of California

Ernest O. Lawrence Radiation Laboratory

PION-MASS MEASUREMENT BY CRYSTAL DIFFRACTION OF MESONIC X RAYS

DISCLAIMER

Submitted to Phys. Rev.

UCRL-16638
preprint

UNIVERSITY OF CALIFORNIA
Lawrence Radiation Laboratory
Berkeley, California

AEC Contract No. W-7405-eng-48

PION-MASS MEASUREMENT BY CRYSTAL DIFFRACTION OF MESONIC X RAYS

Robert E. Shafer

November 2, 1966

Pion-Mass Measurement by Crystal Diffraction of Mesonic X Rays*

Robert E. Shafer†

Lawrence Radiation Laboratory
University of California
Berkeley, California

November 2, 1966

ABSTRACT

The energies of the 4f-3d atomic transitions in pionic calcium and titanium have been measured with a bent-crystal spectrometer, and were found to be 72.352 ± 0.009 and 87.651 ± 0.009 keV, respectively. The relationship of these transition energies to the mass of the negatively charged pion is calculated. Comparison of the measurement with the calculation yields

$$M_{\pi}c^2 = 139.577 \pm 0.013 \text{ MeV}$$

as a new estimate of the charged-pion mass.

Conservation of energy and momentum in the $\pi \rightarrow \mu + \nu$ decay process is examined, and an upper limit of 2.1 MeV (68% confidence level) is assigned to the mass of the muon neutrino.

I. INTRODUCTION

Precision measurement of the energy of an x-ray transition in a pionic (π-mesonic) atom, in combination with a precise calculation of the relationship of this transition energy to the mass of the π^- meson, can yield an accurate estimate of the charged-pion mass. Experiments using this technique were considered more than a decade ago. Early pionic x-ray measurements were able to estimate the π^- mass with about ±0.5% precision. Precise methods such as crystal diffraction of pionic x-rays were considered, but the inherently low efficiency of crystal spectrometers and the low intensity of available pion beams precluded such measurements. Gradual improvement in crystal-diffraction spectroscopy as well as pion-beam facilities has recently made reconsideration of such an experiment worthwhile.

The measurement of two pionic x-rays to approximately ±100 ppm (parts per million) precision with a bent-crystal spectrometer is reported in this paper. The energy-level calculations are carried out to about ±50 ppm precision, leading to a ±100 ppm estimate of the charged-pion mass.

A new measurement of the pion mass is desirable for several reasons. The present best estimates of all the hadron masses depend on measurements of either the pion or proton mass, or both. Some recent hadron mass measurements are of such precision that the existing uncertainty on the pion mass is no longer negligible (e.g., the best present estimate of the charged kaon mass is derived from analysis of $K^+ \to \pi^+ + \pi^+ + \pi^-$ decays[1]). Secondly, combination of a new measurement of the charged-pion mass with other already existing experimental results allows a revision in the upper limit assigned to the mass of the muon neutrino. On the other hand, if the mass of the muon neutrino is assumed to be zero, then these existing experimental results allow an estimate of the π^+ mass with about ±400 ppm precision, which may be directly compared to the measurement of the π^- mass reported here as a test of CPT invariance.

Many measurements of the pion mass have been made previously by other experimental groups using a wide range of techniques. Several experiments are reviewed briefly here to indicate the techniques used, and the range of precision obtainable. A more comprehensive survey is presented in a review article by Barkas.[1]

The Q value of the absorption process $\pi^- + p \rightarrow n + \gamma$ at rest is directly related to the π^- mass. Measurements of the energy of either the 8.8-MeV neutron or the 130-MeV γ ray is sufficient to uniquely determine the pion mass. Crowe and Phillips[2] in 1954 measured the energy of the γ ray with a pair spectrometer, and arrived at an estimate of

$$M_{\pi^-}c^2 = 139.37 \pm 0.20 \text{ MeV}.$$

In 1964, Czirr[3], using time-of-flight techniques to measure the neutron energy, estimated the π^- mass to be

$$M_{\pi^-}c^2 = 139.69 \pm 0.41 \text{ MeV}.$$

Stearns et al.[4] in 1954, by attenuation of several 4f-3d pionic x rays with selected absorption-edge filters, were able to limit the pion mass to the interval

$$139.15 \pm 0.15 < M_{\pi^-}c^2 < 139.76 \pm 0.20 \text{ MeV}.$$

The two most precise estimates of the π^+ mass are derived from emulsion experiments at Berkeley. The development of the mass-ratio technique over a period of several years resulted in the measurement of the π^+ mass by Barkas, Birnbaum, and Smith[5] in 1956. Because the rate of energy loss for charged particles is dependent only on their velocity, the residual ranges of two similarly charged particles with the same initial velocity will be in the ratio of their respective masses. In this experiment, velocity selection was made on the pions and protons by utilizing the cyclotron magnetic field. Measurement of 60 proton and 368 π^+ tracks in emulsion yielded an estimate of (using the present best estimate of the proton mass)

$$M_{\pi^+}c^2 = 139.68 \pm 0.15 \text{ MeV}.$$

A byproduct of this mass-ratio experiment was the measurement of the absolute muon momentum in the decay $\pi^+ \rightarrow \mu^+ + \nu$. Two separate measurements, comprising a total of 364 decays, yielded a combined value of 33.94 ± 0.05 MeV for the $\pi^+ - \mu^+$ mass difference, under the assumption that the muon neutrino has zero mass. Combining this mass difference with the present value of the muon mass ($M_\mu c^2 = 105.659 \pm 0.002$ MeV, from combining the g/m and g-2 measurements[6]) yields an estimate of

$$M_{\pi^+}c^2 = 139.60 \pm 0.05 \text{ MeV}.$$

This has been the accepted value for several years.

A direct measurement of the charged pion mass (i. e., a measurement not based on the assumption $M_{\nu(\mu)} = 0$) allows a check of energy-momentum conservation in $\pi \rightarrow \mu + \nu$ decay. Barkas et al.[5] used this method to assign an upper limit to the mass of the muon neutrino, obtaining

$$M_{\nu(\mu)}c^2 < 3.6 \text{ MeV}.$$

Two other experimental groups have been able to assign precise upper limits to the muon-neutrino mass by energy-momentum conservation in $\mu^+ \rightarrow e^+ + \nu_e + \bar{\nu}_\mu$ decay. Dudziak et al.[7] report an upper limit of

$$M_{\bar{\nu}(\mu)}c^2 < 4.1 \text{ MeV},$$

and Bardon et al.[8] an upper limit of

$$M_{\bar{\nu}(\mu)}c^2 < 2.6 \text{ MeV}.$$

II. PIONIC X-RAY THEORY

A. Introduction

Pionic and muonic x rays have been studied for several reasons, including investigations into atomic physics, nuclear charge distributions, hyperfine-structure effects, and the π-nuclear interaction. They have also been studied with the objective of measuring the pion and muon masses.[4, 9]

In previous mass measurements, the most precise method suitable for "mesonic" x-ray studies was the absorption-edge technique ("mesonic" is used loosely here to include muonic). As the absorption coefficient of an x-ray filter can vary by a large factor in a very small energy interval, precise limits could be placed on the x-ray energies.

Suspicion that the energy of the $3d_{5/2}$-$2p_{3/2}$ muonic phosphorus x ray lay directly on the 100-eV-wide K-absorption edge of lead prompted the most precise "mesonic" x-ray transition-energy calculation to date. In 1959, Petermann and Yamaguchi[10] calculated the quantum-electrodynamic corrections to the Dirac equation for the $3d_{5/2}$ and $2p_{3/2}$ levels of muonic phosphorus,[5] arriving at a relationship between the muonic x-ray energy and the muon mass with a precision of ± 25 ppm. Meanwhile, several experimental groups measured the absorption coefficient of these x-rays in lead. Combination of these data yielded an estimate of the muon mass with a precision of ± 100 ppm which, when compared with a more recent independent measurement of the muon mass (with a precision of ± 15 ppm), verified the muonic x-ray calculations to ± 100 ppm.[6]

The second-order (in e) corrections to the Dirac equation in muonic phosphorous fall into two distinct categories, the virtual production of electron-positron pairs by the Coulomb field (vacuum polarization), and the virtual emission of photons by the muon (Lamb shift). Vacuum polarization, an important correction in "mesonic" atoms, is a correction to the Coulomb field, and hence does not depend directly on the intrinsic properties of the "meson". The Lamb shift, which does depend on the intrinsic properties, may be considered as a short-range effect in "mesonic" atoms, as its "range" is defined by the "meson's" Compton wavelength. It is a negligible correction to "mesonic" atom energy levels except possibly when the effect of a finite nuclear charge distribution is significant.

Pionic and muonic atoms differ in several significant ways. As the pion is a spin-0 particle, the Klein-Gordon equation rather than the Dirac equation must be used. Although the Klein-Gordon equation has not been experimentally verified to the precision required in this paper, the success in understanding the hydrogen atom would make such a verification anticlimactic. Furthermore, pion-nuclear interactions can produce shifts in the atomic energy levels which typically are one or two orders of magnitude larger than the correction for a finite nuclear charge distribution. Nuclear absorption of pions from atomic levels competes with the E1 atomic transitions, resulting in broadening and weakening of the x-ray lines.

The selection of the pionic x-ray lines to be measured with the bent-crystal spectrometer was based on both theoretical and experimental considerations. The corrections to the Klein-Gordon equation had to be estimated to such a precision that the relationship between the pionic x-ray energy and the pion mass would be calculable to about ±50 ppm precision. The important quantum-electrodynamic terms, as mentioned above, have already been adequately tested in electronic hydrogen and muonic phosphorous. The largest uncertainty in the calculation was the estimate of the atomic level shift produced by the π-nuclear interaction. As this could not be calculated to the desired precision from knowledge of the π-nucleon interaction, it was necessary to estimate the level shift from existing experimental data on pionic atoms by perturbation-theory techniques.

Experimental surveys of pionic atoms in the late 1950's[11-13] indicated that the observed strong interaction of pions in 1s orbits decreased the binding energy, and hence was of a repulsive nature. In 1964 a measurement of the 3d-2p pionic aluminum transition[14] indicated that the π-nuclear interaction in 2p orbits increased the binding energy, hence confirming the theoretical prediction that the 3,3 π-nucleon interaction should dominate in $\ell \neq 0$ orbits, giving rise to an attractive force.[15]

The assumption that the π-nuclear interaction is essentially similar in p and d orbits led to the conclusion that the strong interaction shift was calculable to sufficient precision in all 4f-3d pionic transitions for $Z \leqslant 22$. This calculation was based solely on the observed 240 ± 80 eV shift in the 3d-2p pionic aluminum (88-keV) transition. (A recent systematic survey by Jenkins et al.[16] has confirmed the assumptions made here, and has allowed an improvement in the estimates of the strong-interaction shifts required in this paper.)

Consideration of experimental limitations, such as the energy dependence of the spectrometer efficiency and resolution, the Z dependence of the pionic x-ray yield, and the ability to discriminate against background events, led to the selection of calcium ($Z = 20$) and titanium ($Z = 22$) as the most suitable targets for the mass measurement reported here. As will be seen later, measurement of two x-ray lines provides two independent consistency checks on the data.

B. Energy-Level Calculations

The evaluation of the pionic 4f-3d transition energies in calcium and titanium is summarized in Table I. Because the expected experimental precision is of the order of 10 eV, all calculations are rounded off to the nearest eV.

These calculations are based on an origin value of 139.580 MeV for the π^- mass. The origin value divided by the calculated transition energies yields scale factors which to a good approximation are independent of the origin value. Specifically, a 1-MeV shift of the origin value should produce only a 30-ppm effect on the scale factor.

Because pions have no spin, we use the relativistic Schrodinger (Klein-Gordon) equation for a central Coulomb field, described in Section 42 of Schiff.[17] To insure the required precision, the exact solution for the energy levels is used by expanding it in a binomial series and retaining the required number of terms. An expression sufficiently precise for the levels in question is

$$W(n, \ell) = -\left[\frac{1}{2}\left(\frac{\gamma}{\lambda}\right)^2 - \frac{3}{8}\left(\frac{\gamma}{\lambda}\right)^4 + \frac{5}{16}\left(\frac{\gamma}{\lambda}\right)^6\right] M_\pi c^2, \qquad (1)$$

where $\gamma = \alpha Z$ and $\lambda = n-\ell-1/2 + [(\ell + 1/2)^2 - \gamma^2]^{1/2}$. The value[18] $1/\alpha = 137.0388 \pm 4$ ppm was used, its error producing the ± 1 eV error on the calculated energies (note that by using the fine-structure constant, the π^- charge is assumed to be the same as the electronic charge). For titanium, the relativistic shift in the transition energy is about +187 eV (i.e., compared to the nonrelativistic Schrodinger solution). Note that the relativistic correction has introduced a fine structure to the energy levels (i.e., the degeneracy in ℓ has been removed).

The reduced mass correction is[19]

$$E = \frac{W}{1 + M_\pi/M_N} - \left(\frac{Z\alpha}{2n}\right)^2 \frac{M_\pi}{M_N} \left| W \right|, \qquad (2)$$

where W is the energy defined in Eq. (1), E is the "reduced" energy, and (M_π/M_N) is the pion-to-nuclear mass ratio. Note that E and W are both negative energies. The second term, due to nuclear motion, is less than a 0.5 eV effect. For titanium, in which about 25% of the nuclei have A = 46, 47, 49, or 50 (75% is A = 48), the reduced mass correction produces five distinct lines in an energy band about 20 eV wide. Since this band is about 10% of the experimental resolution and about 7% of the reduced mass correction, the effect of the splitting on the analysis is negligible. The weighted average of the isotopic masses is used.

Polarization of the virtual electron-positron pairs produced in the Coulomb field of the nucleus can cause noticeable deviations from the classical Coulomb potential at distances of the order of or less than the electron Compton wavelength ($\hbar/mc \approx 390$ Fermi). This effect, usually referred to as vacuum polarization, was first calculated by Uehling[20] in 1935. This calculation has been checked to ±2% in the hydrogen atom[21] and to ±3% in muonic phosphorous (see Section IIA). For the energy levels of interest here the vacuum-polarization corrections to the energy levels are in the range 0.1 to 0.2%.

Several authors have estimated the second-order vacuum polarization effect in "mesonic" atoms using the Uehling integral in a first-order perturbation-theory calculation with nonrelativistic orbital wave functions.[22-24] In the Appendix this calculation is carried out using relativistic wave functions, yielding a +229.0-eV shift for calcium and a +299.7-eV shift for titanium. Wichmann and Kroll[25] have calculated the corrections to the Uehling integral, and demonstrate that they give rise to an additional shift $\Delta E < 1.9\times 10^{-8} Z^2 \cdot E$, hence < 0.8 eV for the titanium transition. Glauber et al.[26] have corrected the first-order perturbation-theory calculation for the perturbation on the orbital wave function, and find less than a 1-eV effect on the 329-eV vacuum polarization shift in muonic phosphorous. The effect should be quite similar in the pionic atoms considered here. The total second-order vacuum-polarization effect is estimated to be 230 ± 2 eV for calcium, and 301 ± 2 eV for titanium.

The fourth-order vacuum-polarization effect has been calculated by Petermann and Yamaguchi[10] to be approximately 2.9 (α/π) times the second-order effect in muonic phosphorous. By comparison, the ratio in the hydrogen atom is[27] 3.8 (α/π). Assuming the ratio to be about 2.9 (α/π) for the pionic transitions yields a $+2 \pm 2$-eV shift in both calcium and titanium.

The strong-interaction shift is estimated from a recent systematic survey of pionic-atom transition energies by Jenkins et al.[16] Subsequent analysis by Jenkins predicts the shifts to be 2 ± 1 eV for the calcium transition, and 4 ± 2 eV for titanium. The estimate for titanium includes consideration of isotopic effects in the shift.

The effect of atomic electrons penetrating the region of the pionic orbit is easily estimated if we assume that the probability density of the two 1s electrons is a constant in the region of interest. The level shift, relative to the origin, produced in the pionic atom by two 1s electrons, is

$$\Delta E \approx \frac{-4}{3} e^2 \left(\frac{Z-1}{a_0}\right)^3 \langle r^2 \rangle , \qquad (3)$$

where for pionic atoms we have

$$\langle r^2 \rangle = 126 \, (a_\pi/Z)^2 \qquad \text{3d level}$$

$$\langle r^2 \rangle = 360 \, (a_\pi/Z)^2. \qquad \text{4f level}$$

In these expressions a_0 and a_π represent the electronic and pionic Bohr radii, and the factor (e^2/a_0) is 27.2 eV. The overall effect of the electronic screening is to decrease the transition energy (since $|\underset{\sim}{E}(r)| = |dV/dr|$ is reduced everywhere).

In the calcium and titanium transitions this would be a -2-eV effect. However, because the pionic 4f-3d transition is considerably faster than the electronic 2p-1s (E1 radiative transition rates, listed in Bethe and Salpeter,[28] are linear in mass $\times Z^4$), electronic K-shell vacancies produced by preceding pionic Auger transitions will probably not be filled in time. Rather than calculate this small effect, the electronic screening is instead estimated to be -1 ± 1 eV.

Natural linewidths are of the order of several eV, the main contributions coming from the 3d-2p E1 transition rates and the nuclear absorption of pions from the 3d level. The line shapes are expected to be the symmetric Breit-Wigner resonance curves, and therefore do not affect the transition energies.

The short-range electromagnetic effects, including the pion and nuclear form factors and the Lamb shift, are approximately two orders of magnitude smaller than the strong-interaction shift, and therefore are negligible.

Recoil of the pionic atom following the x-ray emission is a -0.1-eV effect and therefore also negligible.

Hyperfine structure is expected in the atoms formed from Ti^{47} ($I = 5/2$, $\mu \approx -0.8\,\mu_N$, $Q \approx 0.2$ barns, natural abundance $\approx 7\%$) and Ti^{49} ($I = 7/2$, $\mu \approx 1.1\,\mu_N$, $Q \approx 0.2$ barns, natural abundance $\approx 5\%$). A d_2 atomic configuration can be split by both M1 and E2 nuclear moments. For the magnetic-dipole interaction, structure is spread over an energy range $\Delta E_\mu \approx 8\mu_N\mu_\pi \langle 1/r^3 \rangle \approx 3$ eV (μ_π is a pion magneton, $\approx 6.7\,\mu_N$), and for the electric quadrupole interaction, $\Delta E_Q \approx 0.5\, e^2 Q \langle 1/r^3 \rangle \approx 50$ eV. The form of these interactions is such that when they are switched on, the center of gravity of the energy spectrum is not shifted. Because ΔE_μ and ΔE_Q are narrower than the experimental resolution [≈210 eV FWHM (full width at half maximum) for the titanium transition], the effect of the hyperfine splitting on the energy-level calculation is negligible.

The transition energy has been calculated for the 4d-3p transition in calcium, and it is found that the effects of the relativistic fine structure, the vacuum polarization, and the π-nuclear interaction are all additive and shift the energy at least 1 keV relative to the 4f-3d transition. Furthermore, the data of Jenkins et al.[16] tentatively indicate the 4d-2p intensity to be about 15% (within a factor of 2) of the 4f-3d in calcium, indicating that the 4d-3p yield is about 5% of the 4f-3d. Therefore, in the data analysis only the 4f-3d line is assumed to be present.

The assigned uncertainties in the calculation of the two scale factors presented in Table I are completely correlated. This correlation is most conveniently handled in the form of an error matrix

$$V_{calc} = \begin{pmatrix} (48\ \text{ppm})^2 & (46\ \text{ppm})^2 \\ (46\ \text{ppm})^2 & (44\ \text{ppm})^2 \end{pmatrix} , \qquad (4)$$

where V_{11} and V_{22} represent the variances of the calcium and titanium scale factors, respectively.

III. THE EXPERIMENT

A. Arrangement

The π^- beam, produced by the circulating internal beam at the 184-Inch Cyclotron, was extracted and transported to the experimental site as illustrated in Fig. 1. The optimum beam momentum was found to be about 180 MeV/c, with a momentum spread $\Delta p/p \approx 7\%$ FWHM. The auxiliary dee facility (actually a cee outside the main dee) was used to provide a uniform spill with a macroscopic duty cycle of about 60%. The microstructure consisted of an 8-nsec pulse every 52 nsec.

The experimental arrangement is illustrated in Fig. 2. A five-counter pion telescope at the focus of a bent-crystal spectrometer detected pions as they stopped in the vicinity of the pionic x-ray target. Behind the spectrometeter, a NaI(Tl) scintillator in fast coincidence with the pion telescope detected x-rays diffracted by the bent crystal.

The bent-crystal spectrometer is a line-source transmission spectrometer, often referred to as being of the DuMond or monochromator geometry. Its long focal length (7.7 m) and large-aperture bent crystal [6-mm-thick quartz (310) crystal with a 160-cm^2 aperture] were chosen specifically for "mesonic" x-ray studies. The instrumental resolution for a thin source is about 17 sec of arc FWHM, which corresponds to a width of 0.63 mm on the focal circle. At 100 keV, the resolution is about 160 eV, and the efficiency about 1.2×10^{-6}, improving to 40 eV and 2.5×10^{-6}, respectively, at 50 keV. A detailed description of this instrument may be found elsewhere.[29]

A detail of the pion telescope is illustrated in Fig. 3. A 1, 2 coincidence was used to monitor the incident beam. The average beam rate was about 1.0×10^{6}/sec, of which about 65% were pions. A suitable range of CH_2 was inserted to stop the pions in the vicinity of the pionic x-ray target. Counter logic $123\bar{4}\bar{5}\bar{C}$ defined the stopping particles. The Čerenkov counter was used to reject electrons, and the threshold of counter 3 was set to detect only heavily ionizing particles (i. e., pions with only a very short residual range). The combination of two anti-counters behind the target--one set to detect heavily-ionizing particles and the other to detect minimum-ionizing particles--was found to be slightly more efficient than a single counter.

The dimensions of the pionic x-ray targets were chosen to be 1.0 by 12.5 by 200 mm^3 for calcium, and 1.0 by 6.5 by 200 mm^3 for titanium. The 1.0-mm dimension slightly compromises the spectrometer resolution in order to obtain a somewhat improved rate of diffracted x-rays. The second dimension of each target is along the bent-crystal line of sight and corresponds to about 0.8 attenuation length for the pionic x rays of interest. For reasons that will be discussed later, increasing this dimension further would adversely affect the data-accumulation rate.

The differential range curve for the degraded pion was about 3.5 g/cm^2 of CH_2 wide, which corresponds approximately to 10 mm of titanium or 20 mm of calcium. The transverse dimensions of the pion beam were about 40 by 130 mm. Hence only a small fraction of the incident pion flux--of the order of 1%--could be stopped in the target material. Although other crystal geometries (i.e., Cauchois or flat-crystal spectrometers) would allow a larger stopping rate since the target would not be at the spectrometer focus, these spectrometers typically exhibit efficiencies about 0.5% that of the DuMond-geometry instruments near 100 keV.

The NaI(Tl) scintillator, whose dimensions were 6.3 by 170 by 170 mm^3, was viewed on one side by nine 2-in.-diam photomultipliers. For an 84-keV nuclear gamma ray (selected from the calibration source by the monochromator), an optimum resolution of 25-keV FWHM was observed. This corresponds statistically to about 0.75 photoelectron per keV of γ-ray energy in the observed pulse. By deriving a timing signal from the arrival of the first photoelectron,[30,31] the overall timing resolution for diffracted x rays in coincidence with stopping pions was expected to be about 8 nsec FWHM (including a 4-nsec quadratic contribution from the pion telescope). The resolution observed during the experiment was about 10 nsec.

Pulse-height analysis, as well as time analysis of the NaI(Tl) signal, was required to separate the real signals from the background, which was due to random coincidences between the NaI(Tl) and the pion telescope. The main source of the singles counting rate in the NaI(Tl) appeared to be from natural radioactivity inside the shielding surrounding it. Turning the cyclotron on and off produced less than a 5% effect on this counting rate. No correlation between the counting rate and the micro- or macrostructure of the beam was observed.

Both a fast signal for time analysis and a linear signal for pulse-height analysis were derived from the NaI(Tl) detector. Figure 4 illustrates the logic used to analyze these pulses. One of the coincidence circuits was timed to detect real, as well as random, events. The other coincidence circuit, essentially identical to the first (both had a resolving time of 14 nsec), was set an integral number of microstructure pulses off-delay to detect only random events. The linear pulses were routed into any of four 100-channel pulse-height analyzers, depending on which logic requirements were satisfied.

Since each pionic x-ray measurement reported here represents several hundred hours of cyclotron time, it was important to include in the experiment proper equipment to monitor the mechanical alignment of the x-ray target and the spectrometer. The autocollimator,[32] shown in Fig. 2, was used for this purpose. The bent-crystal spectrometer, the x-ray target, and the auto-collimator were all mounted on firm concrete foundations in order to minimize relative motion of individual components. An optical target mounted on the bent-crystal form block, together with the autocollimator support, defined a line of sight on which the x ray target was placed. The spectrometer alignment relative to this line of sight was checked by attaching a front-surface mirror to the form block and rotating it into autocollimation with the precision sine screw on the spectrometer. The expected limit on the monitoring of the system alignment was slightly greater than the autocollimator resolution, hence about ±4 sec of arc (As mentioned earlier, the spectrometer resolution is about 17 sec.). During the experiment, specific procedures were used so that misalignments too small to be observed by the optical monitoring equipment would have minimal effects on the final data.

It is worthwhile here to review the efficiency of the system for detecting x-rays. The intrinsic efficiency of the spectrometer for the 88-keV titanium 4f-3d x ray is about 1.3×10^{-6}. However, as the width of the target was slightly larger than the intrinsic resolution, the efficiency averaged over the target width is actually about 9×10^{-7}. The production yield of the 4f-3d x rays is about 0.5 x rays per stopped pion,[33] and only about 70% of these leave the target due to self-absorption. The detection efficiency of the NaI(Tl) is about 0.9. Data analysis also reduces the efficiency in the following way: As mentioned earlier, the timing resolution of the detection system was observed to be about

10 nsec. The resolving time of the coincidence circuits was set to 14 nsec; hence only about 85% of the events were detected by the coincidence circuits, the rest being outside the timing window. A similar reduction also occurs in the pulse-height analysis. This small reduction in counting rate is more than compensated for by a significant increase in the signal-to-background ratio (for the signal-to-background ratio encountered in this experiment, improving it was almost as important as improving the events rate, as far as locating the mean of the diffraction peak was concerned. It was for this same reason that one dimension of the x-ray target was chosen to be 0.8 absorption length). The system efficiency is then about 2×10^{-7} detected x rays per stopped pion in the target.

B. Procedure

The pionic x-ray wavelengths were measured by scanning alternately the regions where the right and left first-order diffraction peaks were expected to be, based on the energy-level calculations. As the angular separation of the two diffraction peaks is measured by the sine-screw mechanism, no reference to the line of sight was required for the wavelength determination. Reference to the line of sight was required only to insure that the diffraction peaks would be situated well within the regions scanned. This alignment was performed with a radioactive source.

In order to minimize the effect of possible long-term relative motion (including any cyclic diurnal motions), of the target and spectrometer on the data, the spectrometer was operated on approximately a 36-hour cycle. Each x-ray measurement consisted of about ten such cycles, so that any unobserved motion (i. e., less than ±4 sec of arc) would have a negligible effect on the data when averaged over all cycles. Thermal expansion of the quartz crystal (about 15 ppm/°C) is an important effect, so the ambient temperature was recorded at regular intervals. (As a comparison, the final wavelength precision quoted for this experiment is about ±100 ppm.).

The net stopping pion rates in the x-ray targets were about 4200 pion/sec in titanium and 3200/sec in calcium, based on target-in-minus-target-out rates and differential range curves. Because the titanium and calcium targets weighed about 6 and 4 g respectively, the stopping pion rate was about 750 pion/g-sec for each target.

As data accumulation progressed, the location of the diffraction peaks were predicted with reasonable precision by χ^2 analysis. Some additional effort was then concentrated on the points that localize the peaks most effectively.

The data thus obtained are illustrated in Figs. 5 and 6. The ordinates represent the events per 10^7 stopping pions, and the abscissae represent the diffraction peak location in units of sine-screw turns from the mechanical center (1 sine-screw turn corresponds approximately to 294 sec of arc). The observed efficiency is seen to be in the range of 1 to 2×10^{-7}, which is consistent with the prediction.

The instrument was calibrated by using the 84-keV nuclear gamma ray ($\lambda = 146.835 \pm 0.005$ xu)[34] and the 52-keV electronic $K_{\alpha 1}$ x ray ($\lambda = 236.165 \pm 0.003$ xu)[35] of a Tm^{170} radioactive source. The quartz-crystal d spacing (at 18° C) was found to be:

Calibration wavelength (xu)	d_{18} Spacing (xu)
147	1177.49 ± 0.06
236	1177.56 ± 0.03

The entire calibration error is contained within the quoted d spacings. The slight deviation between the two measurements is due possibly to a small deviation in the linearity of the sine screw. The calibration is discussed in more detail elsewhere.[29]

From a linear extrapolation between the two calibration points, the calibration values for the two pionic x-rays of interest are:

Transition	Wavelength (xu)	d_{18} Spacing (xu)
Titanium 4f-3d	141	1177.49 ± 0.06
Calcium 4f-3d	171	1177.52 ± 0.05

C. Data Analysis

The intrinsic resolution of the spectrometer has been found to be adequately represented by a Gaussian distribution. For the 1-mm-wide targets used in this experiment the resolution is given by convoluting a Gaussian distribution with (representing the intrinsic resolution) with a rectangle (representing the target), and is closely represented by the function

$$f(\lambda-\lambda_0) = \left[1 + \left(\frac{\lambda-\lambda_0}{a}\right)^2 + \left(\frac{\lambda-\lambda_0}{b}\right)^4\right] \exp\left[-\frac{1}{2}\left(\frac{\lambda-\lambda_0}{c}\right)^2\right], \quad (5)$$

where the constants a, b, and c are known. The resolution for the pionic x-ray lines is 140 eV and 210 eV FWHM for calcium and titanium, respectively.

In the analysis only one diffraction peak is assumed to be present in each spectra (as indicated in section II, the 4d-3p line is expected to be less intense than the 4f-3d by about a factor of 20, for example).

The background under each diffraction peak is assumed to be flat (considering the efficiency of the spectrometer and the lack of any substantial correlation between the NaI(Tl) background counting rate and the cyclotron beam, this is a very reasonable assumption). Hence the expected shape of the spectra is of the form

$$R(\lambda - \lambda_0; N, S) = N + S \cdot f(\lambda - \lambda_0) , \qquad (6)$$

where the noise N, signal S, and wavelength λ_0 remain to be determined.

In the data analysis, the function

$$\chi^2(\lambda_0; N, S) = \sum_i \left[\frac{R(\lambda_i - \lambda_0; N, S) - Y(\lambda_i)}{\sigma_i} \right]^2 , \qquad (7)$$

where $Y(\lambda_i) \pm \sigma_i$, the mean and standard deviation of the ith experimental point, is minimized by computer for each value of the independent variable λ_0 by varying N and S, with the restriction that N and S are greater than zero. The resultant $\chi^2(\lambda_0)$ for the data in Figs. 5 and 6 are plotted in Figs. 7 and 8, respectively. Each of the eight χ^2 curves were analyzed completely independently of one another.

The sum of the four χ^2 minima in Fig. 7 is 31 and in Fig. 8 is 57. The expected value for these sums is $\langle \chi^2 \rangle \pm [2 \langle \chi^2 \rangle]^{1/2} = 42 \pm 9$. If a straight-line fit to the data were attempted, the sums of the minima would be 159 and 66, respectively ($\langle \chi^2 \rangle = 50$ for this case). The only obvious disagreement is for a straight-line fit to the "real" data in Fig. 5. The other χ^2 minima, although not as good as one would like, are nevertheless acceptable.

The ratio $[\chi^2_{min}/\langle \chi^2 \rangle]^{1/2}$ may be shown to be Birge's ratio R,[36] which is a measure of the overall compatibility of the errors assigned to each point with the deviations of the individual points from the minimum χ^2 fit. For the three reasonable χ^2_{min} obtained, Birge's ratio is within about 15% of unity, which may be considered as an estimate of the degree of reliability in the width of the likelihood distribution for the mean of the diffraction peaks.

The relative likelihood distributions for the mean of the four diffraction peaks in Fig. 5 are plotted in Fig. 9. These curves were derived directly from the χ^2 curves in Fig. 7 and were normalized to 1 at the mode. The horizontal error flags represent the mean and standard deviations assigned to each likelihood function. These error flags also appear in Fig. 5. The smooth curves in Fig. 5 correspond to the maximum-likelihood fit, as do the smooth curves in Fig. 6.

The maximum-likelihood estimates of the background level in the four titanium curves in Figs. 5 and 6 are self-consistent, as are the background levels in the calcium data. The height of the two titanium diffraction peaks differ by almost 2 standard deviations. The alignment of the bent-crystal spectrometer components was checked both before and after the experiment and found to be satisfactory, so the only explanation seems to be that the height difference is a statistical fluctuation (≈ 5% probability). This fluctuation is not expected to have any systematic effect on the data analysis, however.

The experimental results are summarized in Table II. As mentioned earlier, 1 sine-screw turn is approximately 294 sec of arc. The midpoints of the two pairs of diffraction peaks differ by 0.009 ± 0.007 sine-screw turns, hence about 2.6 ± 2.1 sec of arc. This is an estimate of the consistency of both sets of data, if we assume the bent-crystal alignment to be identical for both experiments (the other consistency check is the prediction of the π^- mass by each measurement). The sine of the Bragg angle (θ_B) includes a correction for the temperature deviations from 18° C measured during the experiment. The wavelength-to-energy conversion constant used here is 12372.42 xu-keV ± 15 ppm.[35]

The fractional errors quoted for the two x-ray energies each represent a standard deviation of ± 9 eV. These errors are partially correlated, the error matrix for the two energy measurements being

$$V_{exp} = \begin{pmatrix} (127\ \text{ppm})^2 & (48\ \text{ppm})^2 \\ (48\ \text{ppm})^2 & (99\ \text{ppm})^2 \end{pmatrix}, \qquad (8)$$

where V_{11} and V_{22} represent the variance of the calcium and titanium measurements, respectively.

IV. CONCLUSIONS

A. The Negative-Pion Mass

The product of the measured transition energies in Table II and the calculated scale factors in Table I yields the following estimates for the π^- mass:

Transition	π^- Mass Estimate
Calcium 4f-3d	139.582 MeV ± 136 ppm
Titanium 4f-3d	139.574 MeV ± 109 ppm.

The error matrix for the two measurements is, from Eqs. (4) and (8),

$$V = V_{calc} + V_{exp} = \begin{pmatrix} (136\ \text{ppm})^2 & (66\ \text{ppm})^2 \\ (66\ \text{ppm})^2 & (109\ \text{ppm})^2 \end{pmatrix}, \qquad (9)$$

where the off-diagonal elements contain contributions from the spectrometer calibration, the energy-level calculation, and the wavelength-energy conversion factor.

The weighted average of the two measurements is[37]

$$M_{\pi^-} c^2 = 139.577 \text{ MeV} \pm 96 \text{ ppm},$$

where

$$\left[\sum_i (V^{-1})_{ij}\right]^{-1/2} = 96 \text{ ppm} \Rightarrow 0.013 \text{ MeV}.$$

This estimate agrees with the previous measurements described in Section I. If the muon neutrino mass is assumed to be zero, the π^+-to-π^- mass ratio is found to be 1.0002 ± 0.0004. Hence there does not appear to be any evidence of CPT nonconservation in the charged pion mass at the level of precision attained here. (As a comparison, the μ^+-to-μ^- mass ratio is observed to be 1.0000 ± 0.0001.)

Note added in proof: A very recent measurement of h/e by the Josephson effect[38] (still in progress) is yielding values of the fine-structure constant about 21 ± 5 ppm below the accepted value. The authors show that this would raise the present best estimate of the electron mass (and hence also the muon mass) by about 63 ppm. It is therefore relevent to discuss the dependence of the present pion mass measurement on h/e and α.

The pion mass estimate is obtained by comparing the <u>wavelength</u> of a pionic x ray to a calibration wavelength λ_c. The measured wavelength is converted to an energy using the energy-wavelength conversion constant $V\lambda_s = c^2h/\Lambda e$. This x-ray energy is in turn related to the pion mass through a function of α^2. Specifically:

$$M_{\pi}c^2 \propto \frac{V\lambda_s}{\lambda_c} \alpha^{-2} = \frac{c^2}{\lambda_c \Lambda}\left(\frac{h}{e}\alpha^{-2}\right), \tag{10}$$

where terms of higher order in α have been neglected. But

$$\frac{h}{e}\alpha^{-2} = \frac{c}{2R_{\infty}\gamma_p} \frac{\mu_p}{\mu_0} , \tag{11}$$

where c is the velocity of light, R_{∞} is the Rydberg constant for infinite mass, γ_p is the proton gyromagnetic ratio, and μ_p/μ_0 is the proton magnetic moment in Bohr magnetons. These constants allow determination of $(h/e)\alpha^{-2}$ to about ±3 ppm, independent of existing measurements of either h/e or α (further discussion of this point is presented elsewhere[39]).

B. The Muon-Neutrino Mass Limit

As demonstrated by Barkas et al.,[5] an upper limit on the muon-neutrino mass may be assigned by applying energy-momentum conservation in $\pi \to \mu + \pi$ decay. For decay at rest (c = 1 units) we have

$$M_{\nu}^2 = (M_{\pi} - M_{\mu})^2 - 2M_{\pi}T_{\mu} , \tag{12}$$

where T_{μ} is the kinetic energy of the recoil muon in the c.m. system of the pion. The best present values for the input parameters are (it is assumed here that the π^+ and π^- masses are equal):

$M_{\pi} = 139.577 \pm 0.013$ MeV (this experiment)

$M_{\mu} = 105.659 \pm 0.002$ MeV (Feinberg and Lederman)[6]

$P_{\mu} = 29.80 \pm 0.06$ MeV (Barkas et al.)[5].

The latter two combine to yield $T_{\mu} = 4.122 \pm 0.016$ MeV. The standard deviations of the first and second terms of Eq. (12) are due almost entirely to M_{π} and T_{μ} respectively, and therefore are essentially uncorrelated. A graphical solution of Eq. (12) is illustrated in Fig. 10. The likelihood distribution for M_ν^2 (which is Gaussian in units of M_ν^2) is found by projecting the bivariate distribution onto the M_ν^2 axis.

The likelihood distribution in M_ν^2 represents the relative likelihood that a neutrino of mass M_ν would have produced the observed experimental result. The a priori assumption that the neutrino mass is contained within the interval $0 \leq M_\nu^2 < \infty$ is quite reasonable, as negative values of M_ν^2 are associated with velocities greater than c. So the distribution is normalized such that the likelihood of the neutrino mass being in the interval $0 \leq M_\nu^2 < \infty$ is 100%. Analysis of this distribution then yields the upper limits

$$0 \leq |M_\nu| < 2.1 \text{ MeV} \qquad 68\% \text{ confidence}$$

$$0 \leq |M_\nu| < 2.7 \text{ MeV} \qquad 90\% \text{ confidence.}$$

Other estimates of the muon-neutrino mass are reviewed in Section I.

Referring again to Fig. 10, it is apparent that improvements in the estimates of the pion and muon masses will not significantly modify the present limit on the muon-neutrino mass, but that a new precise measurement of T_μ (or P_μ) could reduce the upper limit to about 1 MeV.

ACKNOWLEDGMENTS

The author is very grateful to Professor Kenneth M. Crowe for his continuing support and encouragement throughout the author's career as a graduate student.

The experiment described herein was originally proposed in 1957 by Professor J. W. M. DuMond (California Institute of Technology) and Professor Crowe.

The assistance offered during the experiment by Dr. David Jenkins, as well as contributions made to earlier phases of the pionic x-ray program at Berkeley by Dr. A. Astbury, Dr. J. P. Deutsch, and Dr. R. Taylor is gratefully acknowledged.

The cooperation of James T. Vale and the cyclotron crew in operating and maintaining the 184-inch Cyclotron near its peak efficiency contributed significantly to the success of the experiment.

It was a pleasure to have the opportunity to discuss the physics of mesonic atoms with Professor Robert Karplus, Professor Charles Schwartz, Professor Evyind Wichmann, and Professor Emilio Segrè.

APPENDIX

A. Vacuum Polarization Shift Using Relativistic Wave Functions

The relativistic radial wave equation for a spinless particle in a central Coulomb field is (from Section 42 of Schiff)[17]

$$\frac{1}{\rho^2}\frac{d}{d\rho}\left(\rho^2\frac{dR}{d\rho}\right) + \left(\frac{\lambda}{\rho} - \frac{1}{4} - \frac{\ell(\ell+1) - \gamma^2}{\rho^2}\right) R = 0, \qquad \text{(A-1)}$$

where $\gamma = \alpha Z$, $\lambda = n - \ell - 1/2 + [(\ell + 1/2)^2 - \gamma^2]^{1/2}$, $\rho = 2kr$, and $k = (\hbar c)^{-1} [(M_\pi c^2)^2 - E^2]^{1/2}$; E = total energy.

Substituting $R(\rho) = \rho^s e^{-\rho/2} u(\rho)$, where $s = \lambda - n + \ell$, we have

$$\rho u'' + [2(s+1) - \rho] u' - [s + 1 - \lambda] u = 0. \qquad \text{(A-2)}$$

Making the substitution $b = 2(s+1)$ and $a = s + 1 - \lambda$

$$\rho u'' + (b - \rho) u' - a u = 0.$$

The solution is the confluent hypergeometric function as described in Section 20 of Schiff.[17] For circular orbits we have $\ell = n - 1$, and hence $s = \lambda - 1$ and $a = 0$. The normalized solution which is regular at $r = 0$ is then

$$R(r) = \left[\frac{8\,k^3}{\Gamma(2\lambda+1)}\right]^{1/2} (2kr)^{\lambda-1} e^{-kr}. \qquad \text{(A-3)}$$

In the nonrelativistic limit this reduces to the hydrogen-atom radial wave functions, (i.e., $\lambda \rightarrow n$ and $k \rightarrow Z/na_\pi$ where a_π is the Bohr radius).

The second-order vacuum-polarization shift from first-order perturbation theory is

$$\Delta E = -e \langle R | \Delta\phi | R \rangle \qquad \text{(A-4)}$$

$$= -Ze^2 \langle R | \frac{1}{r} \left(\frac{\Delta\phi}{\phi_c}\right) | R \rangle.$$

Where

$$\frac{\Delta\phi}{\phi_c} = \left(\frac{\alpha}{3\pi}\right)\int_1^\infty \frac{e^{-2\mu r x}(x^2-1)^{1/2}(2x^2+1)}{x^4}\,dx$$

is the Uehling integral,[20] where $\mu = mc/\hbar$ is the inverse electron Compton wavelength. Integration over r yields

$$\Delta E = -\left(\frac{\alpha}{3\pi}\right)\frac{Ze^2k}{\lambda}\int_1^\infty \frac{(x^2-1)^{1/2}(2x^2+1)}{x^4\left(1+\frac{\mu x}{k}\right)^{2\lambda}}\,dx, \qquad \text{(A-5)}$$

which reduces to the expression derived by Mickelwait[23] and Koslov[24] in the nonrelativistic limit. The substitution $x = 1/v$ yields

$$\Delta E = -\left(\frac{\alpha}{3\pi}\right)\frac{Ze^2k}{\lambda}\int_0^1 \frac{(1-v^2)^{1/2}(2+v^2)\,v^{2\lambda-1}}{\left(v+\frac{\mu}{k}\right)^{2\lambda}}\,dv, \qquad \text{(A-6)}$$

which is more suitable for computer evaluation.

In particular, for the 4f-3d transitions in pionic calcium and titanium (using a reduced mass derived from $M_\pi c^2 = 139.58$ MeV) we obtain the following values:

	Vacuum polarization shift (eV)	
Energy Level	Relativistic	Nonrelativistic
Calcium 3d	-316.4	-315.1
Calcium 4f	- 87.4	- 87.2
Titanium 3d	-420.1	-418.1
Titanium 4f	-120.4	-120.0

FOOTNOTES AND REFERENCES

*This work was performed under the auspices of the U. S. Atomic Energy Commission.

†Now at the Laboratory for Nuclear Science, Massachusetts Institute of Technology, Cambridge, Massachusetts.

1. W. H. Barkas, Ann. Rev. Nucl. Sci. 15, 67 (1965).
2. K. M. Crowe and R. H. Phillips, Phys. Rev. 96, 470 (1954). These authors and those of Refs. 5 and 35 have chosen to express their statistical errors in units other than standard deviations. Assuming a normal error curve, we have reexpressed their deviations as a standard error in this paper.
3. J. B. Czirr, Phys. Rev. 130, 341 (1963).
4. M. Stearns, M. B. Stearns, S. DeBenedetti, and L. Leipuner, Phys. Rev. 95, 1353 (L) (1954).
5. W. H. Barkas, W. Birnbaum, and F. M. Smith, Phys. Rev. 101, 778 (1956). See also Ref. 2.
6. G. Feinberg and L. M. Lederman, Ann. Rev. Nucl. Sci. 13, 431 (1963).
7. W. F. Dudziak, R. Sangane, and J. Vedder, Phys. Rev. 114, 336 (1959).
8. M. Bardon, P. Norton, J. Peoples, A. M. Sachs, and J. Lee-Franzini, Phys. Rev. Letters 14, 449 (1965).
9. J. Rainwater, Ann. Rev. Nucl. Sci. 7, 1 (1957).
10. A. Petermann and Y. Yamaguchi, Phys. Rev. Letters 2, 359 (1959).

11. S. DeBenedetti, Nuovo Cimento (10) 4, Suppl., 1209 (1956).

12. D. West, Rept. Progr. Phys. 21, 271 (1958).

13. M. B. Stearns, Progr. Nucl. Phys. 6, 108 (1957).

14. A. Astbury, J. P. Deutsch, K. M. Crowe, R. E. Shafer, and R. E. Taylor, Compt. Rend. Congr. Intern. Phys. Nucl. 2, 225 (1964). See also, Bull. Am. Phys. Soc. 9, 393 (1964).

15. M. Ericson and T. E. O. Ericson, Ann. Phys. (N. Y.) 36, 323 (1966). Earlier work is cited in this reference.

16. D. A. Jenkins and K. M. Crowe, Phys. Rev. Letters 16, 637 (1966); D. A. Jenkins and R. Kunselman, Phys. Rev. Letters 17, 1148 (1966); and D. A. Jenkins, private communications (1965 and 1966).

17. L. I. Schiff, Quantum Mechanics (McGraw Hill Book Co., New York, N. Y., 1949).

18. E. R. Cohen and J. W. M. DuMond, Rev. Mod. Phys. 37, 537 (1965).

19. The nuclear motion term is derived for the Dirac atom case by H. A. Bethe and E. E. Salpeter in Quantum Mechanics of One and Two Electron Atoms, (Academic Press, New York, 1957). As the result is dependent on only the orbital quantum number n, it is assumed that the same term also applies to a Klein-Gordon atom.

20. E. A. Uehling, Phys. Rev. 48, 55 (1935).

21. G. W. Erickson and D. R. Yennie, Ann. Phys. (N. Y.) 35, 271 (1965). See also R. T. Robiscoe and B. L. Cosens, Phys. Rev. Letters 17, 69 (1966) and M. F. Soto, Phys. Rev. Letters 17, 1153 (1966).

22. L. Foldy and E. Eriksen, Phys. Rev. 95, 1048 (1954).

23. A. B. Mickelwait, thesis, Carnegie Institute of Technology, 1954 (unpublished); A. B. Mickelwait and H. C. Corben, Phys. Rev. 96, 1145 (1954).

24. S. Koslov, thesis, Nevis Cyclotron Laboratory Report No. 19, 1956 (unpublished). See also Ref. 9, p. 17.

25. E. Wichman and N. Kroll, Phys. Rev. 101, 843 (1956).

26. R. Glauber, W. Rarita, and P. Schwed, Phys. Rev. 120, 609 (1960).

27. M. Baranger, F. Dyson, and E. Salpeter, Phys. Rev. 88, 680 (1952).

28. Ref. 19, page 266.

29. K. M. Crowe and R. E. Shafer, Rev. Sci. Instr. 38, 1 (1967).

30. R. F. Post and L. I. Schiff, Phys. Rev. 80, 1113 (L) (1950).

31. L. G. Hyman, Rev. Sci. Instr. 36, 193 (1965).

32. The alignment telescope was a Keuffel and Esser Model 71-2022 with an angular magnification of 47X and a resolving power of 3.4 sec of arc.

33. Y. Eisenberg and D. Kessler, Phys. Rev. 123, 1472 (1961).

34. F. Boehm and C. Gunther, private communication (1965), obtained an energy of 84.261 ± 0.003 keV for this line. I. Marklund and B. Lindstrom, Nucl. Phys. 40, 329 (1963) obtained a value of 84.260 ± 0.004 keV (their original value, 84.262 ± 0.004 keV, has been modified due to a reevaluation of their calibration line[35]).

35. J. A. Bearden, U. S. A. E. C. Report NYO-10586 (1964), (unpublished). See also Ref. 2.

36. See p. 580 of Ref. 18.

37. This estimate is 0.003 MeV lower than the preliminary estimate by R. E. Shafer, K. M. Crowe, and D. A. Jenkins, Phys. Rev. Letters 14, 923 (1965).

38. W. H. Parker, B. N. Taylor, and D. N. Langenberg, Phys. Rev. Letters 18, 287 (1967).

39. Ibid., equation (2).

Table I. Calculations of the 4f-3d pionic calcium and titanium transition energies with $M_{\pi}c^2$ = 139.580 MeV.

Effect	Transition energy (keV) Calcium	Titanium
Klein-Gordon equation	72.388 ± 0.001	87.622 ± 0.001
Reduced mass	- 0.270 ± 0.001	- 0.273 ± 0.001
Vacuum polarization (second-order)	+ 0.230 ± 0.002	+ 0.301 ± 0.002
Vacuum polarization (fourth-order)	+ 0.002 ± 0.002	+ 0.002 ± 0.002
Strong-interaction shift	+ 0.002 ± 0.001	+ 0.004 ± 0.002
Orbital-electron screening	- 0.001 ± 0.001	- 0.001 ± 0.001
Electromagnetic form factors	negligible	negligible
Lamb shift	negligible	negligible
Pionic-atom recoil	negligible	negligible
Hyperfine effects	negligible	negligible
Calculated transition energy	72.351 ± 0.003 keV	87.655 ± 0.004 keV
Scale factor: $\frac{M_{\pi}c^2}{\text{transition energy}}$	1929.21 ± 48 ppm	1592.38 ± 44 ppm

Table II. Experimental results.

Parameters	Calcium diffraction peaks: Left	Calcium diffraction peaks: Right	Titanium diffraction peaks: Left	Titanium diffraction peaks: Right
"Signal" events in peak	176	199	341	375
"Signal"/"background" ratio	0.58	0.77	0.80	1.23
Signal events rate at mode ($hour^{-1}$)	2.3	2.6	2.3	3.0
Total running time (hours)	-------320-------		------360------	
Diffraction-peak location (sine-screw turns)	-50.6829±0.0089	+51.5585±0.0068	-41.7517±0.0057	+42.6462±0.0042
Midpoint (sine-screw turns)	+0.438 ± 0.006		+0.447 ± 0.004	
Separation (× 0.5) (sine-screw turns)	51.1207 ± 0.0056		42.1989 ± 0.0036	
Sine θ_B (at 18° C)	0.0726120 ± 119 ppm		0.0599388±84 ppm	
Wavelength (xu)	171.004 ± 126 ppm		141.155 ± 98 ppm	
Energy (keV)	72.352 ± 127 ppm		87.651 ± 99 ppm	

FIGURE LEGENDS

Fig. 1. The π^- beam-transport system.

Fig. 2. The experimental arrangement.

Fig. 3. Detail of the pion telescope, Counter logic $123\bar{4}\bar{5}\bar{C}$ defined a pion stopping in the vicinity of the x-ray target. Counters 1, 2, and 3 are 20 cm high, and $\bar{4}$, $\bar{5}$, and $\bar{C}$, 25 cm.

Fig. 4. Block diagram of the logic for analyzing the NaI(Tl) pulses.

Fig. 5. Events rate for the "real" data, plotted against the setting of the bent-crystal spectrometer measured in sine-screw turns (1 sine-screw turn is about 294 sec of arc). The smooth curves represent maximum-likelihood fits, and the horizontal error flags represent the mean and its standard deviation for each diffraction peak, as determined by χ^2 analysis.

Fig. 6. Events rate vs spectrometer setting for the "random" data.

Fig. 7. χ^2 values for fitting the expected line shape to the "real" data in Fig. 5. The expected value of χ^2 is indicated.

Fig. 8. χ^2 values for fitting the expected line shape to the "random" data in Fig. 6. The data show essentially no structure, although the χ^2 minima are slightly larger than expected [the expected value of χ^2 in each curve is the same as that for the corresponding curve in Fig. 7.].

Fig. 9. Relative-likelihood distributions for the means of the diffraction peaks in Fig. 5. These curves are derived directly from the χ^2 data in Fig. 7. The horizontal error flags represent the mean and standard deviation for each curve.

Fig. 10. Graphical solution to Eq. (12), using the best estimates of the experimental parameters (c = 1 units). All projections of the bivariate distribution are Gaussian. The largest single contribution to the error on M_ν comes from T_μ.

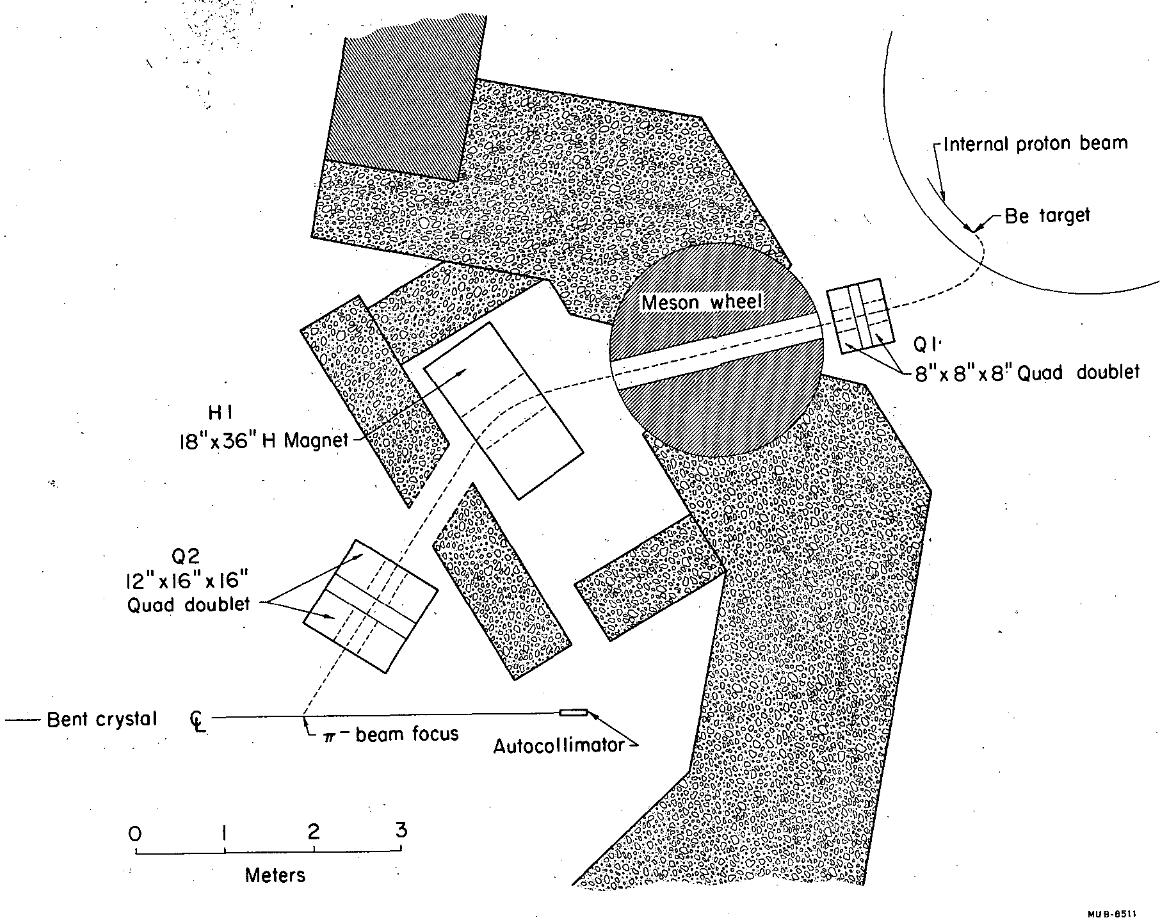

Internal proton beam
Be target
Meson wheel
Q1
8"x8"x8" Quad doublet
H1
18"x36" H Magnet
Q2
12"x16"x16"
Quad doublet
Bent crystal
℄
π⁻ beam focus
Autocollimator
0
1
2
3
Meters
MUB-8511

Fig. 1.

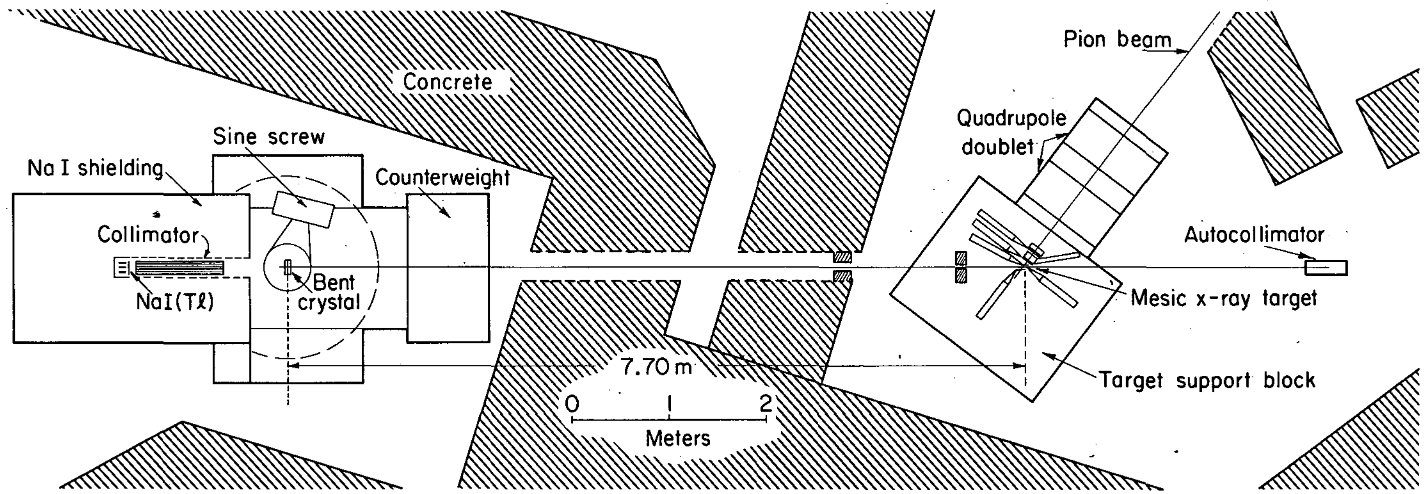

MUB-6014

Fig. 2.

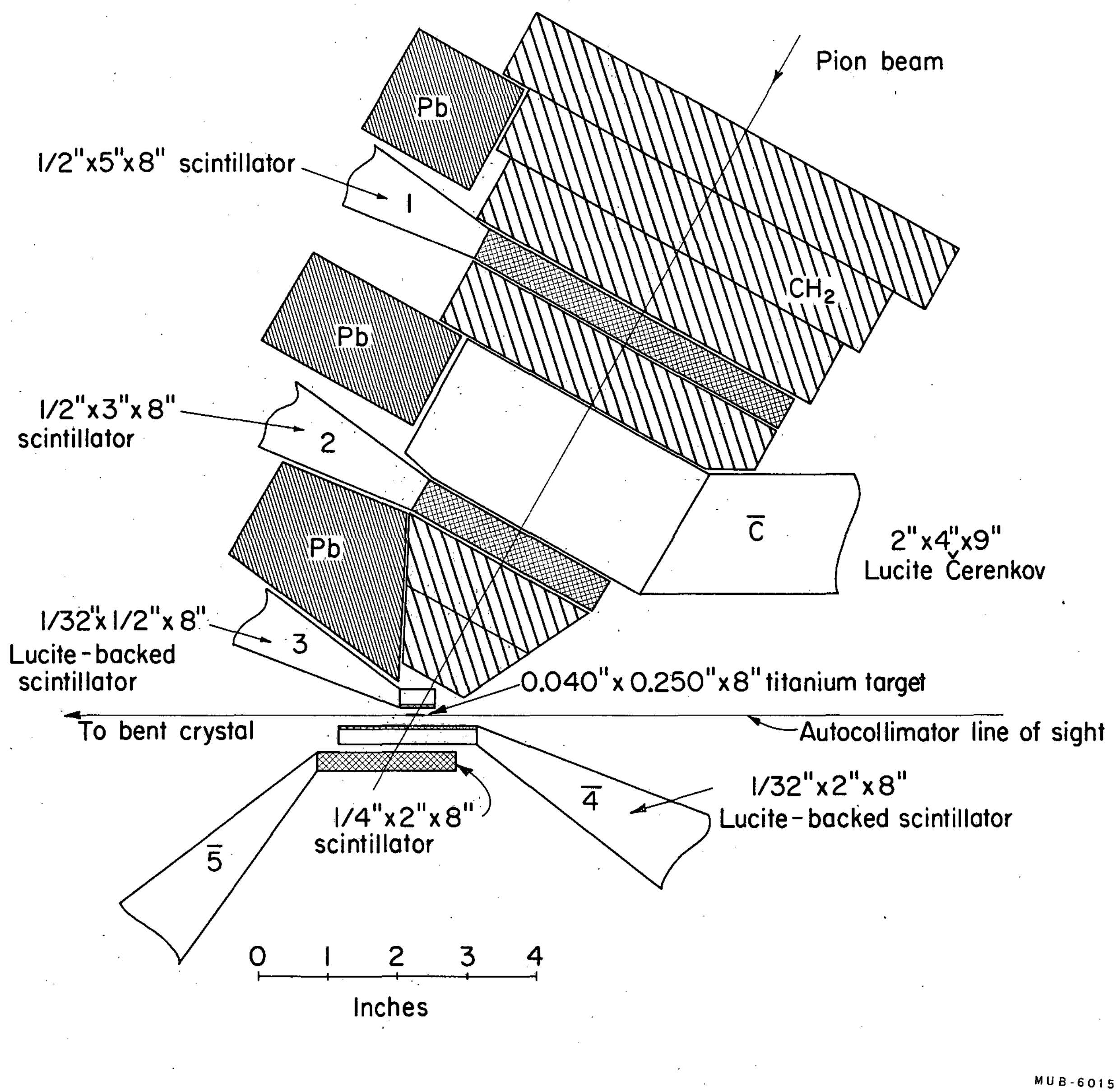
Pion beam
Pb
1/2"x5"x8" scintillator
1
CH₂
Pb
1/2"x3"x8"
scintillator
2
Pb
C̄
2"x4"x9"
Lucite Čerenkov
1/32"x1/2"x8"
Lucite-backed
scintillator
3
0.040"x0.250"x8" titanium target
To bent crystal
Autocollimator line of sight
1/32"x2"x8"
Lucite-backed scintillator
4̄
1/4"x2"x8"
scintillator
5̄
0 1 2 3 4
Inches
MUB-6015

Fig. 3.

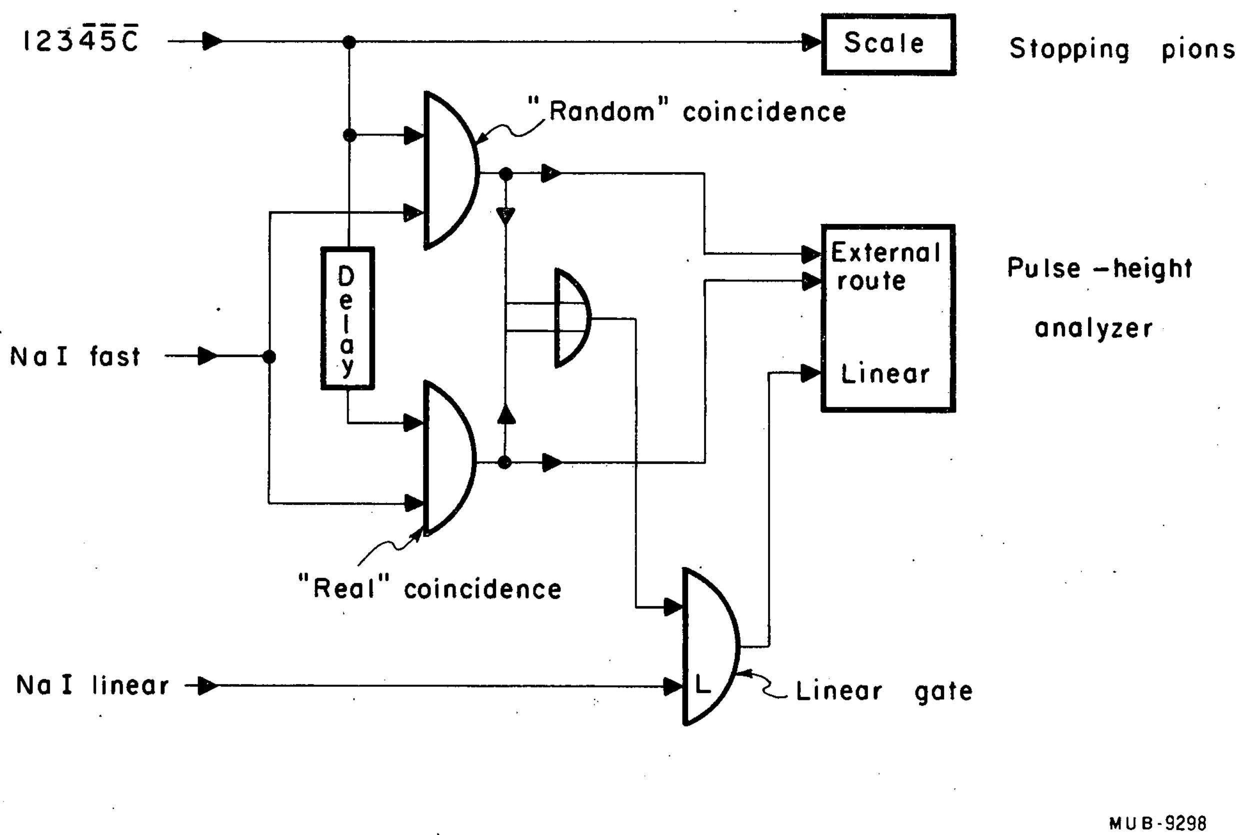
12345C
Scale
Stopping pions
"Random" coincidence
External route
Linear
Pulse-height analyzer
D e l a y
NaI fast
"Real" coincidence
NaI linear
L
Linear gate
MUB-9298

Fig. 4.

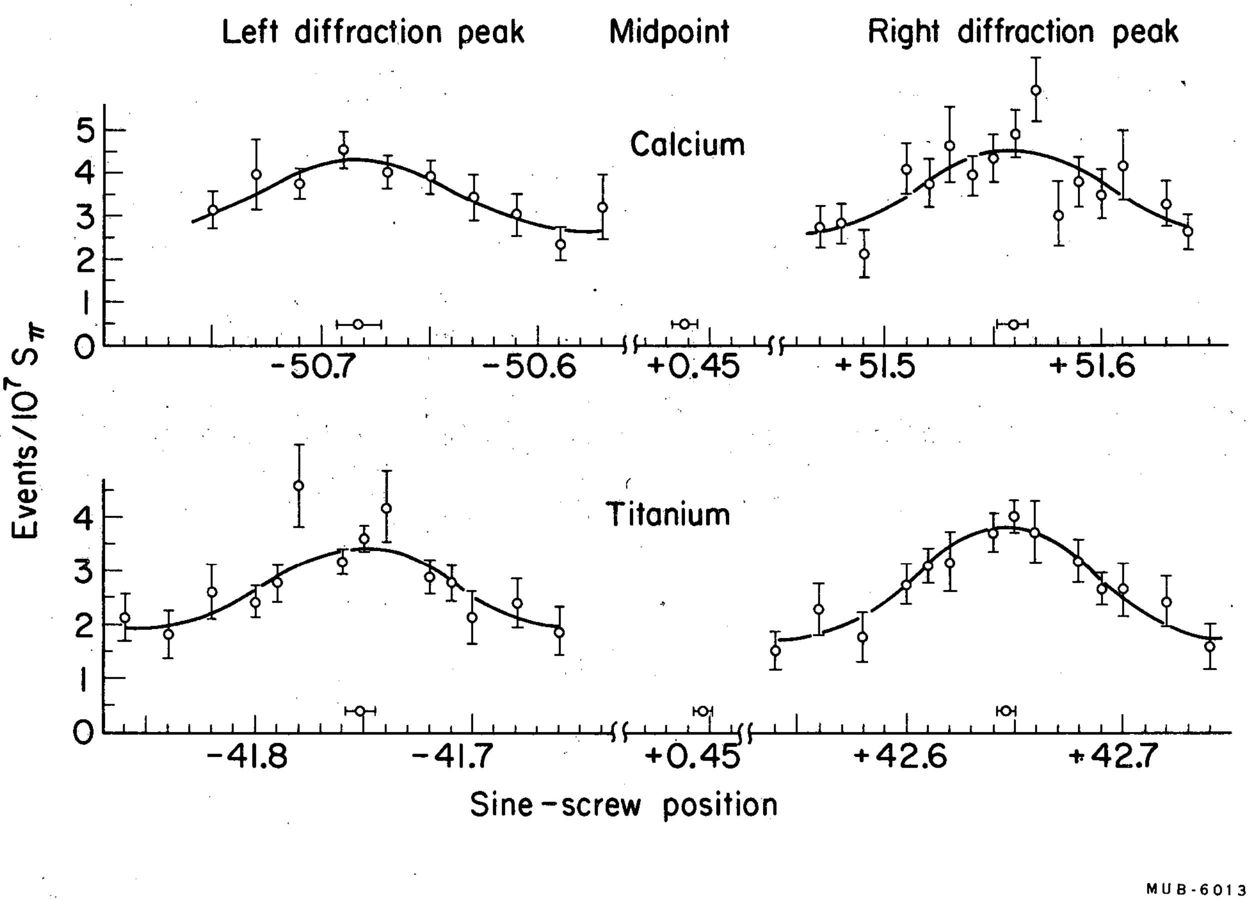

Left diffraction peak
Midpoint
Right diffraction peak
Calcium
Titanium
Events/10^7 S$_\pi$
-50.7
-50.6
+0.45
+51.5
+51.6
-41.8
-41.7
+0.45
+42.6
+42.7
Sine-screw position
MUB-6013

Fig. 5.

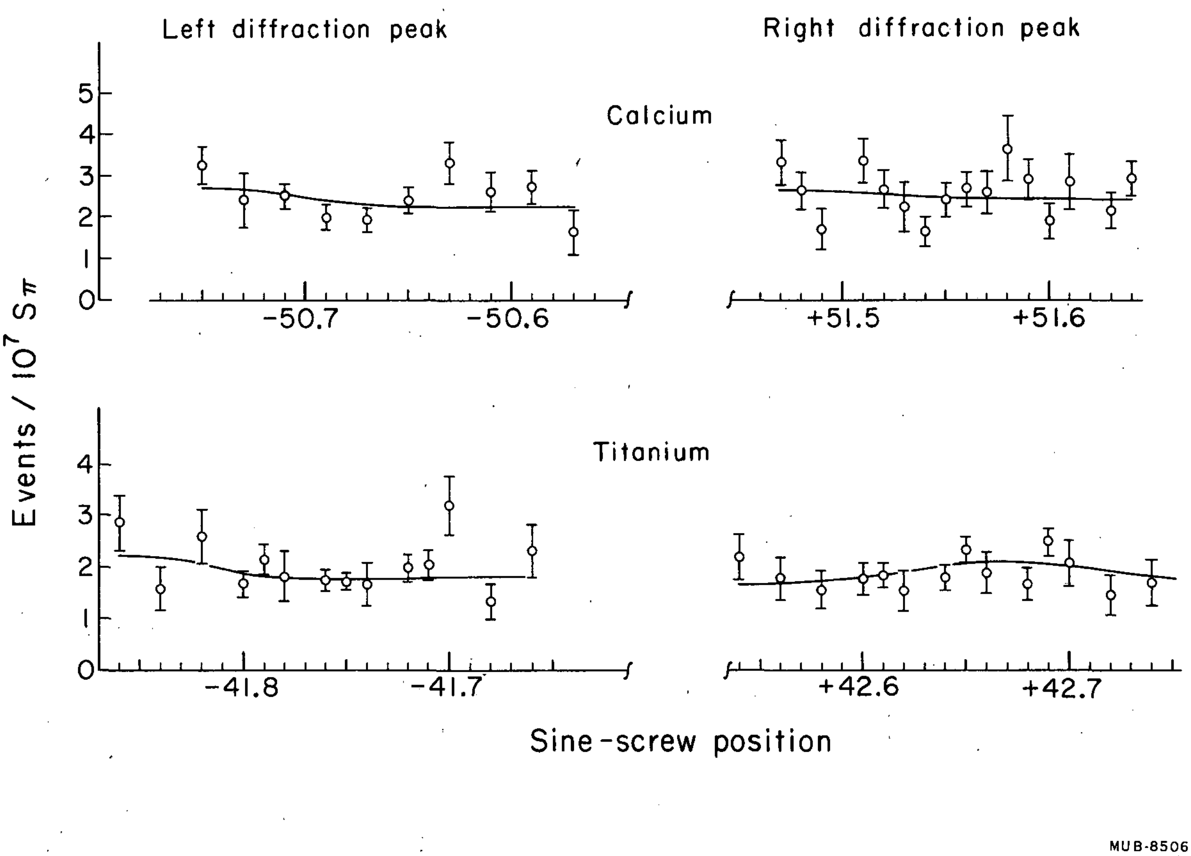
Left diffraction peak
Right diffraction peak
Calcium
Titanium
Events / $10^7 S_\pi$
5
4
3
2
1
0
-50.7
-50.6
+51.5
+51.6
-41.8
-41.7
+42.6
+42.7
Sine-screw position
MUB-8506

Fig. 6.

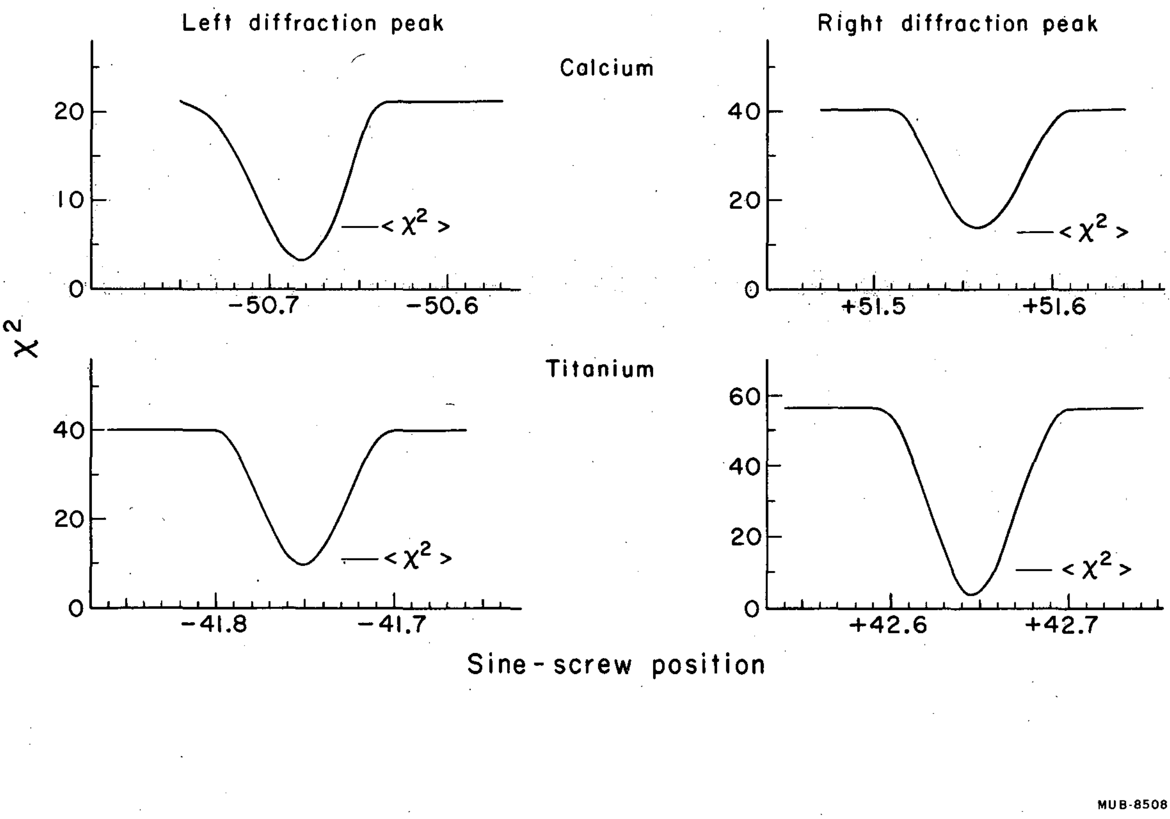
Left diffraction peak
Right diffraction peak
Calcium
Titanium
χ^2
$<\chi^2>$
20
10
0
-50.7
-50.6
40
20
0
+51.5
+51.6
40
20
0
-41.8
-41.7
60
40
20
0
+42.6
+42.7
Sine-screw position
MUB-8508

Fig. 7.

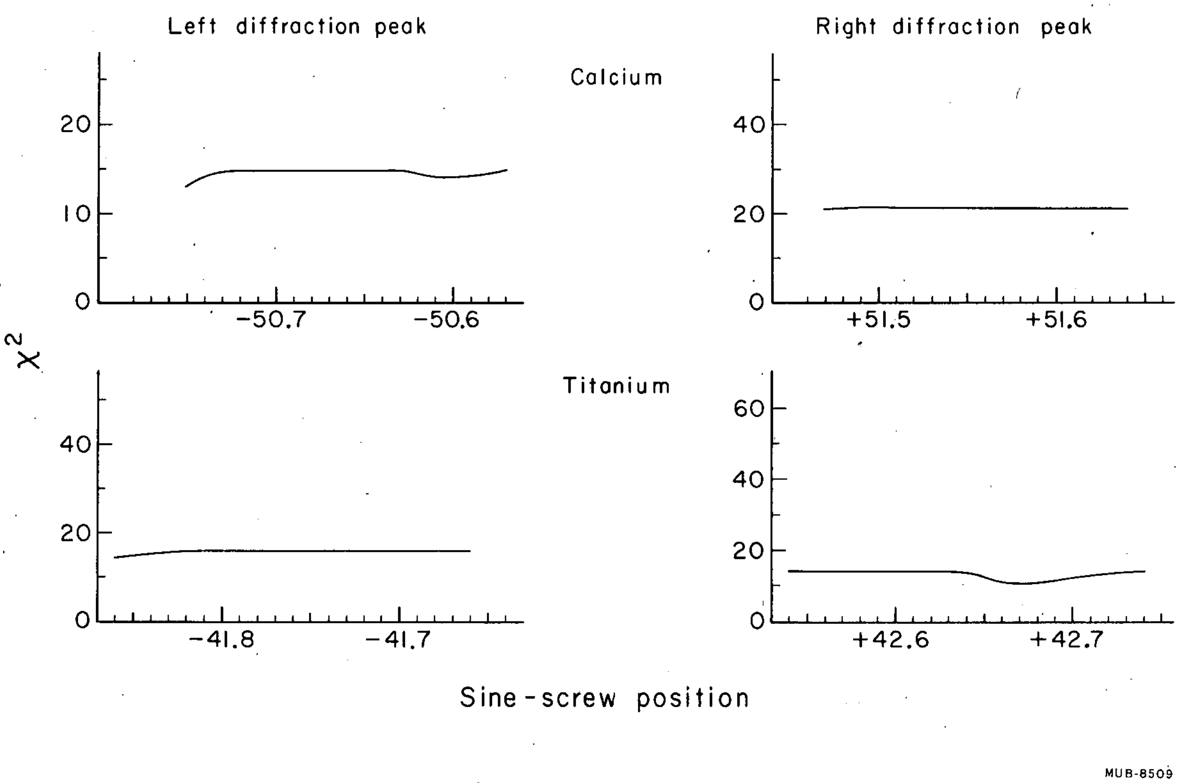
Left diffraction peak
Right diffraction peak
Calcium
Titanium
χ^2
20
10
0
-50.7
-50.6
40
20
0
+51.5
+51.6
40
20
0
-41.8
-41.7
60
40
20
0
+42.6
+42.7
Sine-screw position
MUB-8509

Fig. 8.

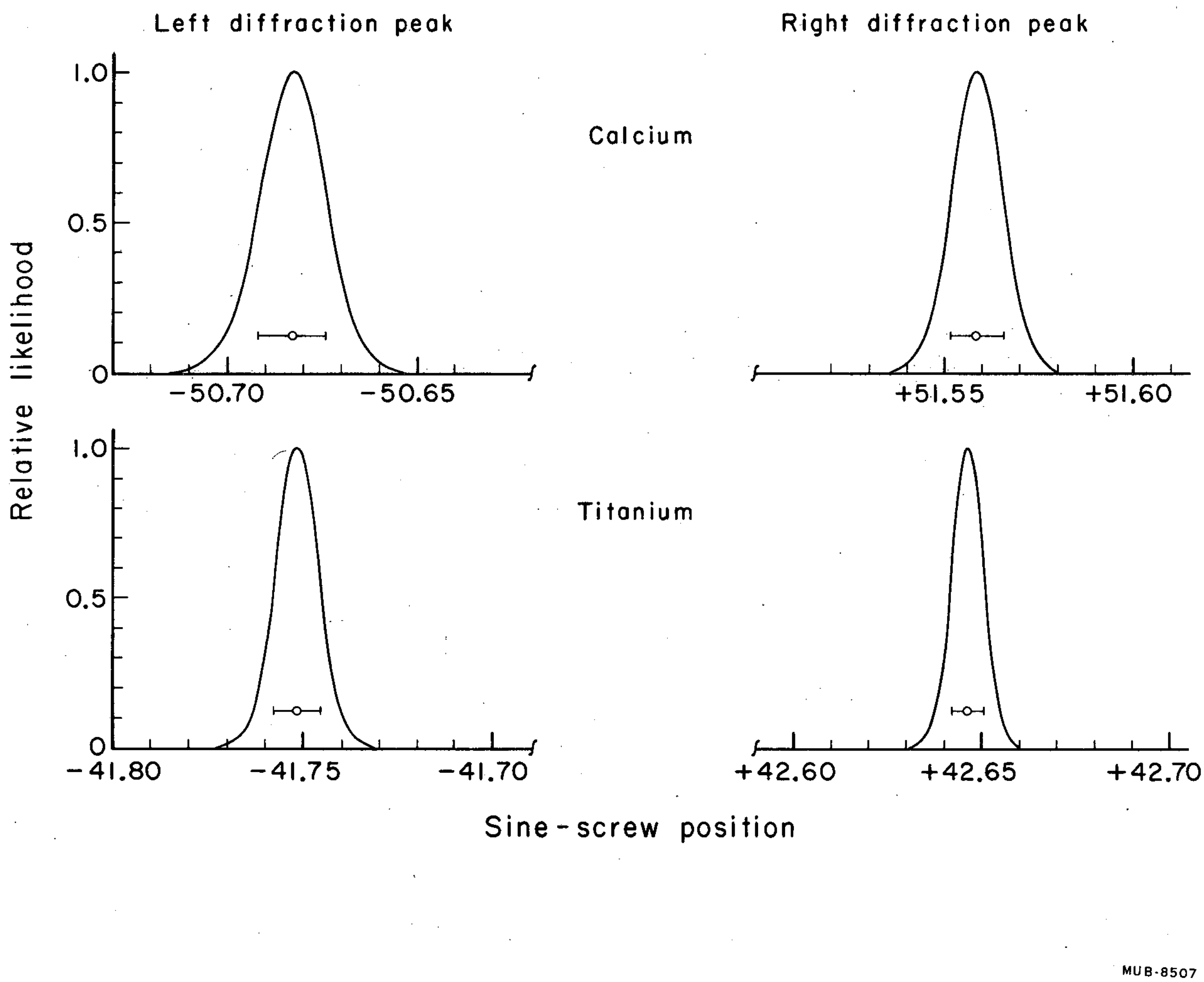
Left diffraction peak
Right diffraction peak
Calcium
Titanium
Relative likelihood
1.0
0.5
0
-50.70
-50.65
+51.55
+51.60
-41.80
-41.75
-41.70
+42.60
+42.65
+42.70
Sine-screw position
MUB-8507

Fig. 9.

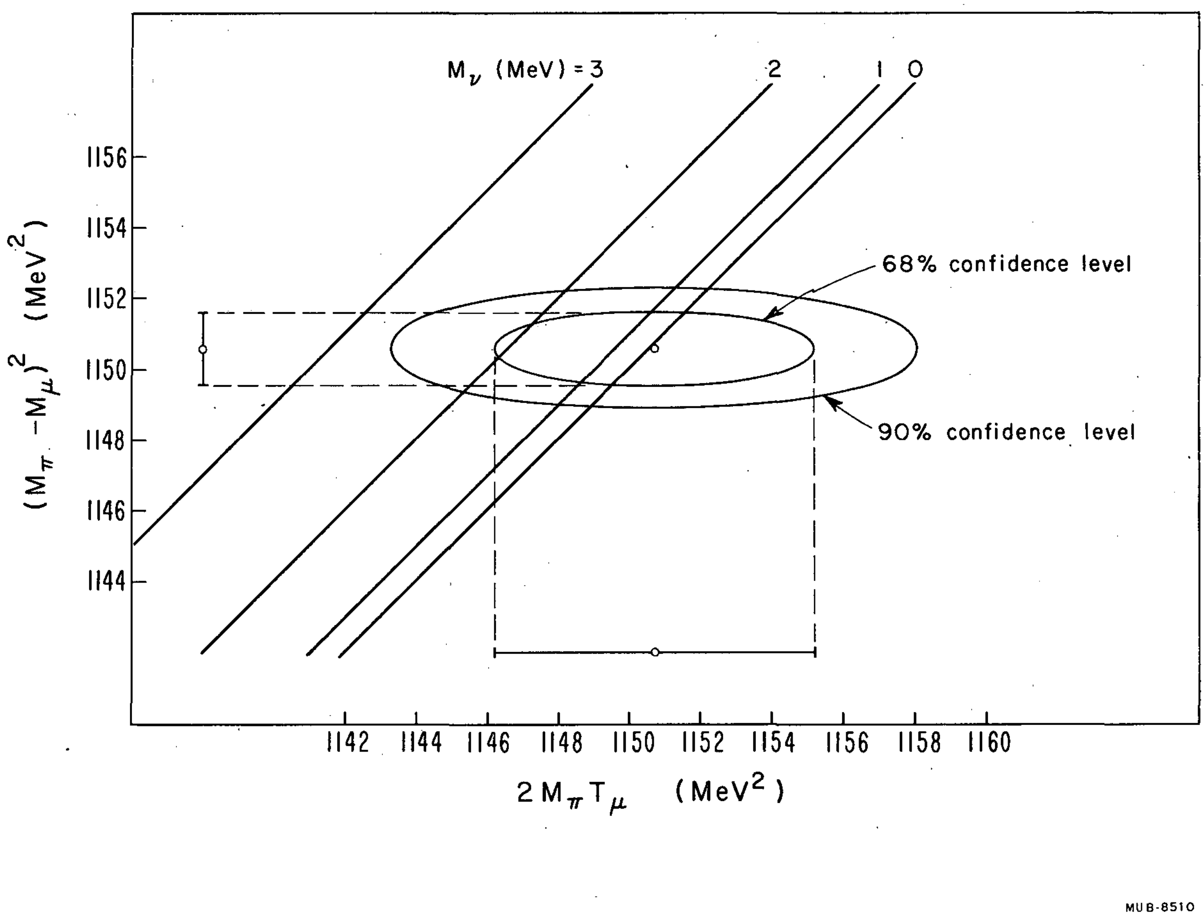
M_ν (MeV) = 3
2
1
0
68% confidence level
90% confidence level
1156
1154
1152
1150
1148
1146
1144
$(M_\pi - M_\mu)^2$ (MeV^2)
1142
1144
1146
1148
1150
1152
1154
1156
1158
1160
$2 M_\pi T_\mu$ (MeV^2)
MUB-8510

Fig. 10.